Express Polymer Letters Vol.17, No.7 (2023) 738–758
Available online at www.expresspolymlett.com
https://doi.org/10.3144/expresspolymlett.2023.55

Research article

The influence of entanglements of macromolecules on the mechanical and thermal properties of polylactide composites with carbon nanotubes

*Hoorieh Barangizi, Justyna Krajenta, Andrzej Pawlak**

Centre of Molecular and Macromolecular Studies, Polish Academy of Sciences, Sienkiewicza 112, 90-363 Lodz, Poland

Received 24 January 2023; accepted in revised form 31 March 2023

Abstract. The influence of the reduction of macromolecular entanglements on the thermal and mechanical properties of polylactide composites containing 0.1–1.0 wt% of carbon nanotubes was investigated. Partial disentangling of the macromolecules improved the dispersion of the filler during composite fabrication. Greater mobility of less entangled polylactide macromolecules affected the crystallization of nanocomposites, which occurred already during the cooling of the melt and not only as a cold crystallization. Isothermal crystallization studies showed a beneficial combination of matrix disentanglement and increased nanotube nucleation, leading to much faster crystallization. In the entangled composite, crystallization at 120 °C was completed after 14 min, while in the partially disentangled composite only after 9 min. The reduction of entanglements of macromolecules also affected the mechanical properties. The plastic deformation was more easily initiated, and stresses in the strain-hardening phase increased more slowly during the deformation of disentangled homopolymers. In composites, the strain-hardening effect depended not only on the content of nanotubes but also on their dispersion, which was better in the less entangled polylactide matrix.

Keywords: *nanocomposites, mechanical properties, thermal properties, disentangling*

1. Introduction

Polylactide (PLA) is an aliphatic polyester derived from renewable resources. It has been intensively explored because it is non-toxic to the human body, friendly to the environment, and compostable [1]. Polylactide can occur in the form of two stereoisomers, designated as L and D, but is usually a mixture of them. When the content of the minor enantiomer does not exceed a few percent, the polymer is capable of crystallization. Usually, it does not occur directly during cooling from the melt but during increasing the temperature in the solid state, as the so-called cold crystallization [2, 3]. Polylactide is brittle under typical exploitation conditions, *i.e.*, below a glass transition at 56–58 °C. However, at temperatures above 60 °C, it is possible to obtain large deformations.

One of the possible ways to improve the unsatisfactory properties of biopolymer is to make a composite. The effective fillers are multi-walled carbon nanotubes (MWCNT). The properties of PLA/MWCNT composites were studied by many authors [4, 5]. The research focused mainly on two issues: thermal properties, including crystallization, and mechanical properties.

Many studies have focused on the crystallization of composites [6–13]. Some of them are concerned with non-isothermal crystallization. The tested composites were able to crystallize when cooled, which resulted in cold crystallization observed in PLA but not in PLA/MWCNT [6]. Different were the observations by Park *et al*. [9], where only a decrease in the cold crystallization temperature (T_{cc}) and an increase

*Corresponding author, e-mail: andrzej.pawlak@cbmm.lodz.pl

in the melt crystallization temperature were observed as a result of increasing carbon nanotubes (CNTs) content in the composite. Rizvi *et al*. [10] noted that a decrease in T_{cc} is observed for CNTs concentration below 2 wt% because highly concentrated MWCNTs inhibit the growth of PLA crystals and increase this temperature. Similar to changes in T_{cc}, the melting temperature of the composites changed. The glass transition temperature (T_g) usually was constant, although Wu and Liao [11] noticed an increase in T_g with the addition of CNTs.

According to Wu *et al*. [13], the presence of nanotubes has a nucleating effect on both the melt crystallization and the cold crystallization of PLA. However, the nanotubes also act as a physical barrier, hindering crystal growth [12]. As a result, the presence of nanotubes accelerated the melt crystallization while retarded the overall kinetics of the cold crystallization. The heat of melting of PLA in the composite regularly decreased with the CNTs content [11].

Xu *et al*. [7] noticed for MWCNTs with a modified surface that, if they have a smaller aspect ratio, the nucleation rate of PLA spherulites increases. It was attributed to fewer sidewall carboxyl groups on the surfaces of MWCNTs with smaller aspect ratios, which provides more nucleation sites for PLA crystallization. The increase in PLA crystallinity after modification of MWCNTs compared with the composite of unmodified MWCNTs and the double melting behavior for nanocomposites, while the pure PLA showed a single melting character, were the main observations of Mina *et al*. [8].

Isothermal crystallization studies showed that the insertion of CNT effectively increased the crystallization rate of PLA [9]. Also, for carboxyl-functionalized MWCNTs composite, the effect of nanotubes on the isothermal cold crystallization of PLA was observed [12].

The mechanical properties of PLA/MWCNT composites are essential for practical applications; therefore, they have been studied by several teams. Some of them observed an increase in tensile strength with an increase in the content of nanotubes [14], but other authors did not find such dependence [15]. It was also found that the flexural strength of the composite increased with MWCNTs content [14]. The mechanical properties of composites depended on the shape of the filler. Composites with a higher aspect ratio were characterized by a higher modulus and higher tensile strength, which was related to the better dispersion of CNTs [16].

Studies of the properties of composites with chemically modified CNTs lead to the general conclusion that the modification of mechanical properties is most effective when the chemical treatment of CNTs improves their dispersion [11, 17–19]. It was found that the tensile strength of PLA/CNT composite was enhanced when a small number of modified MWCNTs was added to PLA [8, 9]. The observations of changes in the modulus of elasticity were contradictory. Ramontja *et al*. [17] noted that Young's modulus of the composite is lower than that of pure PLA, but Chiu *et al*. [20], Park *et al*. [9], and Mina *et al*. [8] reported the opposite tendency.

In all of the above studies, the mechanical properties were determined at 20–25 °C, which meant that PLA was rigid even after CNTs were applied, so only minimal tensile deformation of the composite was possible.

Since the properties of PLA composites depend on the dispersion of CNTs, it was investigated how the dispersion depends on extrusion parameters [21]. In processing, it is recommended to use masterbatches. The MWCNTs dispersion within the diluted composites was predominated by the filler dispersion in the masterbatches. The high rotational speed – in combination with a screw profile containing mainly mixing elements – was found to be very suitable for the dispersion and distribution of MWCNTs. The temperature profile applied showed less influence.

The polymers that make the composites have entangled macromolecules in the amorphous phase [22]. These macromolecular entanglements significantly affect the behavior of not only the deformed polymer but also its composite. It is assumed that in a typically synthesized polymer, macromolecular entanglements are at an equilibrium level characteristic of each polymer [23, 24]. The entanglement density of macromolecules is characterized by giving the average molecular mass between the entanglements. Values in the range of 4000–10 500 g/mol are given in the literature for polylactide [24, 25].

It is possible to reduce the density of entanglements, and appropriate methods have been developed [25]. The reduction of entanglements can be achieved by polymerization occurring together with crystallization. For commercially available polymers, entanglements can be reduced by dissolution. The more the polymer solution is diluted, the less contact there is

between macromolecules and their entanglement. A certain difficulty is to maintain limited entanglements when converting the polymer from solution to solid state. This is often achieved by freezing the solution and sublimating the solvent or precipitating it with a non-solvent. The ability of the polymer to crystallize when the solution is cooled may also be useful in maintaining disentanglement.

Disentangling polymers in solution is well suited for scientific purposes. However, in industrial applications where the environmental aspect must be taken into account, it would be better to achieve the disentanglement of macromolecules in a different way. Recently, attempts have been made to disentangle macromolecular chains using large-amplitude oscillatory shear flow [26]. It should be noted that a fully disentangled polymer is not of interest as a material because the entanglements ensure the continuity of the amorphous phase during deformation. At the same time, the partial reduction of the entanglement density is interesting because, as has been shown for many polymers, it significantly affects their properties [27, 28].

Attempts were made to partially disentangle polylactide macromolecules, similarly to a number of other polymers [24, 29–31]. The rheological experiments showed that polylactide obtained from 0.1 wt% methylene chloride solution has only 20% of the original entanglements. The crystallization studies under isothermal conditions have shown that crystal growth can be 10% faster in partially disentangled PLA. Shifts in temperatures defining crystallization regimes were also observed [31]. The role of chain entanglements in the crystallization of stereocomplex of partially disentangled PLA enantiomers was studied by Sun *et al*. [32]. It was observed that disentangling promoted not only a higher crystallization rate but also higher crystallinity of the complex in both the non-isothermal and isothermal conditions. The less-entangled samples crystallized exclusively as the highly crystalline stereocomplexes, in contrast to the predominant homo crystallization that occurred in the common entangled samples.

The tensile test of mechanical properties showed that plastic deformation is easier in the partially disentangled polymer. This was particularly evident as a decrease in strain hardening rate because, during the final strain phase the deformation is mostly controlled by entanglements in the amorphous phase [33].

Although there are already many reports on the properties of partially disentangled polymers, there are almost no such studies in the case of polymer composites. An exception is a recently published article by Barangizi and Pawlak [34] discussing the crystallization of polypropylene in a composite with 1 wt% dispersed nano Al_2O_3. It was found that isothermal and non-isothermal crystallization occurs faster or at a higher temperature, respectively, if the composite has fewer macromolecular entanglements. This was evident during the measurements of the spherulite growth rate as well as the rate of melt-crystal conversion. However, the crystallization in the nanocomposite was slower than in the homopolymer because the dispersed nanoparticles hindered the movement of macromolecules to the growing crystals.

Luo *et al*. [35] studied the recovery of entanglements in polypropylene with graphene nanoplates and noticed that the presence of graphene increases the rate of crystallization. Drakopoulos *et al*. [36] prepared from a solution a composite of gold nanoparticles dispersed in partially disentangled ultra-high molecular weight polyethylene (UHMWPE). The composite was then calendered and stretched to draw ratios ranging from 2–200. Thus, the processability of UHMWPE was shown. As a result of the deformation, an increase in UHMWPE crystallinity by 15% was found at high drawing ratios. It was also observed that the average size of the gold aggregates increased with the orientation of the composite. Studies of polyethylene with polyhedral oligomeric silsesquioxanes [37, 38] lead to the conclusion that sufficiently small nanoparticles (*e.g.*, 1.5 nm, smaller than the tube size of polyethylene (PE), equal to 3.6 nm) can result in higher free volume in the melt, less chain entanglement, and thus a lower complex viscosity of polymer matrix. The distribution of TiO_2 nanoparticles in waterborne acrylic copolymer coatings caused a chain disentanglement and an order of magnitude decrease of T_g [39].

As can be seen from the above review of the literature, there are no reports that would allow a complete assessment of how the reduced density of macromolecular entanglement affects the formation and properties of composites. Particularly interesting are composites with fillers having a high aspect ratio, well dispersing in the polymer matrix, and characterized by sufficient adhesion to the matrix polymer. To carry

out the relevant research on composite with partially disentangled macromolecules, we chose PLA/MWCNT composite, focusing on its most important properties, *i.e.* thermal and mechanical.

2. Experimental

2.1. Materials

Poly(L-lactide) NW 4032D by Nature Works was used in the research. It contained only 1.15% of D-lactide, so it was able to crystallize. Molecular weight measurements by gel permeation chromatography with multi-angle laser light scattering detection (GPC–MALLS) gave the following values: number average molecular weight, M_n = 72 000 g/mol, mass average molecular weight, M_w = 88 000 g/mol. Thin multi-walled carbon nanotubes were produced by Nanocyl S.A. (Belgium) using a catalytic chemical vapor deposition (CCVD) process. According to the manufacturer's data, NC 7000 nanotubes have an average diameter of 9.5 nm, length of 1.5 μm, and surface area of 250–300 m^2/g.

2.2. Methods

The partial disentangling of PLA was done in solution using a procedure similar to that proposed by Liu *et al*. [30]. PLA – after drying for 4 hours at 70 °C – was dissolved in methylene chloride at a concentration of 0.5% by weight. Mixing of the polymer and solvent was carried out in a glass flask with a mechanical stirrer for 40 min at 25 °C. The homogeneous solution was slowly poured into a large volume of liquid nitrogen. In the next step, ethanol was added to the frozen solution in a volume five times the volume of the solution. This resulted in the precipitation of polylactide as a white powder. Finally, residual methylene chloride and ethanol were removed by drying for about 8 hours under a vacuum at room temperature. Previously performed rheological studies showed that by using this procedure, the molecular mass between entanglements increased from 10 500 g/mol for the original PLA to 32 800 g/mol for the solution-treated PLA. This means three times fewer entanglements in the polymer.

Both fully entangled and partially disentangled PLA was used to prepare composites with MWCNTs. The composites were produced using EHP-5CS mini extruder (Zamak-Mercator, Krakow, Poland). The plasticizing system of this extruder was composed of two screws with a variable profile and a return channel with a valve, enabling multiple passages of the material through the extruder. The components were mixed for 10 min at a temperature of 180 °C with screw rotation of 60 rpm. The composites of entangled or partially disentangled PLA, including 0.1 or 1.0 wt% of MWCNTs, were prepared. It is assumed that to obtain the desired properties of nanocomposites, the content of 1 wt% of the filler should be sufficient. On the other hand, it was difficult to predict whether effects related to the disentanglement of the composite matrix would be visible at a very low content of CNTs. Therefore, the contents of 0.1 and 1.0 wt% CNTs were selected for the study. We did not modify the surface of the filler. Although it could improve the dispersion of nanotubes, it would make it difficult to interpret the impact of reducing macromolecular entanglements on the morphology of the nanocomposite and its properties. Therefore, the modification of the filler-polymer interactions was abandoned, but we paid attention to whether a satisfactory dispersion of the filler was achieved in the mixing process.

The morphologies of the composites were observed with a polarized light microscope Nikon Eclipse 80i (Nikon Corp., Japan). The aim of the research was to analyze the filler dispersion. The samples for observation were prepared on a Linkam TAHMS 600 (Linkam Sci., Salfords, United Kingdom) hot stage. A small piece of the composite was placed between two thin microscopic glasses. Then, such a sandwich was put on the plate of the hot stage, melted for 1 min at 220 °C, and gently compressed into a layer with a thickness of 12–14 μm. The molten film was quickly cooled to room temperature, thereby limiting crystallization and making it transparent for observation. The samples prepared in this way were observed in the microscope in the light transmission mode. Fragments of samples with typical dispersion of filler were photographed. Each of the five photographs taken for each material covered an area of 0.6×0.9 mm. From these photographs, histograms that show the frequency of occurrence of agglomerates of a certain size in each composite were determined. Observations of the morphology of the composites at higher magnification were carried out using a scanning electron microscope (SEM) Jeol JSM 6010LA (JEOL Ltd., Japan). The samples for observation were first broken in liquid nitrogen, and then the exposed surfaces were sputtered with gold. DSC Q 20 (TA Instruments, New Castle, USA) apparatus was used to conduct thermal tests on samples

having a weight 7–8 mg. For the non-isothermal test, the sample was heated to 220 °C at a rate of 10 °C/min, cooled to 25 °C at the same rate, and then heated to 220 °C. In isothermal tests, the sample was heated to 220 °C, kept there for 3 min, and then cooled down at the rate of 10 °C/min to the final temperature of 120 or 125 °C. While maintaining this temperature, changes in heat flow were observed. The experiment was stopped when heat changes became invisible.

The thermogravimetric analyzer TGA 5500 (TA Instruments, New Castle, USA) was used to assess the thermal stability of the tested materials. Examined samples were heated at a rate of 10 °C/min under nitrogen flow from 20 to 600 °C, and weight changes were measured.

The samples for the mechanical test were prepared by hot pressing pieces of composites or polylactides at 180 °C for 6–8 min. Plates with a thickness of 1 mm were obtained, from which samples were cut. The specimens had a gauge length of 25 mm, a width of 10 mm, and a thickness of 1 mm. Five samples of each material were prepared for testing. The samples were tested in a tensile mode using the Instron 5582 (Instron, Norwood, USA) universal machine. The experiments were carried out in an environmental chamber, which enabled the tests to be conducted at temperatures of 20–70 °C. The stretching rate was 10%/min. Changes in the shape of the samples during deformation were recorded by photographs. Markers were drawn on the surface of the samples, which helped to determine local changes in dimensions. By measuring the sizes for a selected small volume between the markers, the volume strain ΔV as a function of the strain was calculated. The volume strain is defined as (Equation (1)):

$$\Delta V = \frac{V - V_0}{V_0} \tag{1}$$

where V_0 is the initial volume of the analyzed fragment of the sample, and V is the actual volume of this fragment. The large value of ΔV is attributed to the occurrence of cavitation phenomena [40]. Micrometer-size cavities (voids) appear in the amorphous phase of the polymer. The intensity of the phenomenon decreases with temperature when the possibility of stress relaxation in the amorphous phase of the polymer increases. The tensile experiment was limited to the engineering strain of 400–500% due to the size of the environmental chamber. Most of the samples tested at 70 °C did not break at these strains.

X-ray scattering, resulting from structural changes in deformed samples, was investigated in the small angle X-ray scattering (SAXS) experiment. The GeniX Xenocs (Xenocs, Grenoble, France) X-ray source operating at 50 kV and 1 mA was combined with a Kiessig-type SAXS camera of 1.2 m in length. The scattered radiation was recorded using a Pilatus 100 K detector. The investigated samples had similar thicknesses.

The formation of the crystalline phase due to the deformation of the stretched material was investigated by recording 2-dimensional wide-angle X-ray scattering (WAXS) patterns. The radiation source was a CuK_α lamp (sealed tube operating at 30 kV and 50 mA, by Philips). The deformed sample from the mechanical test was placed in the path of the X-ray beam at a distance of 39 mm from the Pilatus 100K detector, which recorded the scattering image.

The dynamic mechanical analyzer DMA Q800 (TA Instruments, New Castle, USA) was used to determine how the storage and loss moduli of the PLA sample change with temperature. The test specimens in the shape of strips had the following dimensions: length 10 mm, width 6 mm, and thickness 0.25 mm. The experiments were performed in the film tension mode. Measurements were carried out in the temperature range of 10–160 °C, at a frequency of 1 Hz and a scanning rate of 3 °C/min. The choice of the maximum temperature resulted from the expected melting of the samples above it.

Abbreviations of material names used in the text are presented in Table 1.

3. Results and discussion

3.1. Morphologies of composites

Before carrying out the thermal and mechanical tests, the dispersion of nanotubes in the polymer matrix was evaluated. It is almost impossible to avoid the presence of individual large agglomerates of filler in

Table 1. Abbreviations of material names used in the text.

Material	PLA matrix	MWCNT contents [wt%]
PLAi	Initial PLA, fully entangled macromolecules	0
PLAi 0.1		0.1
PLAi 1.0		1.0
PLAd	Solution treated, partially disentangled macromolecules	0
PLAd 0.1		0.1
PLAd 1.0		1.0

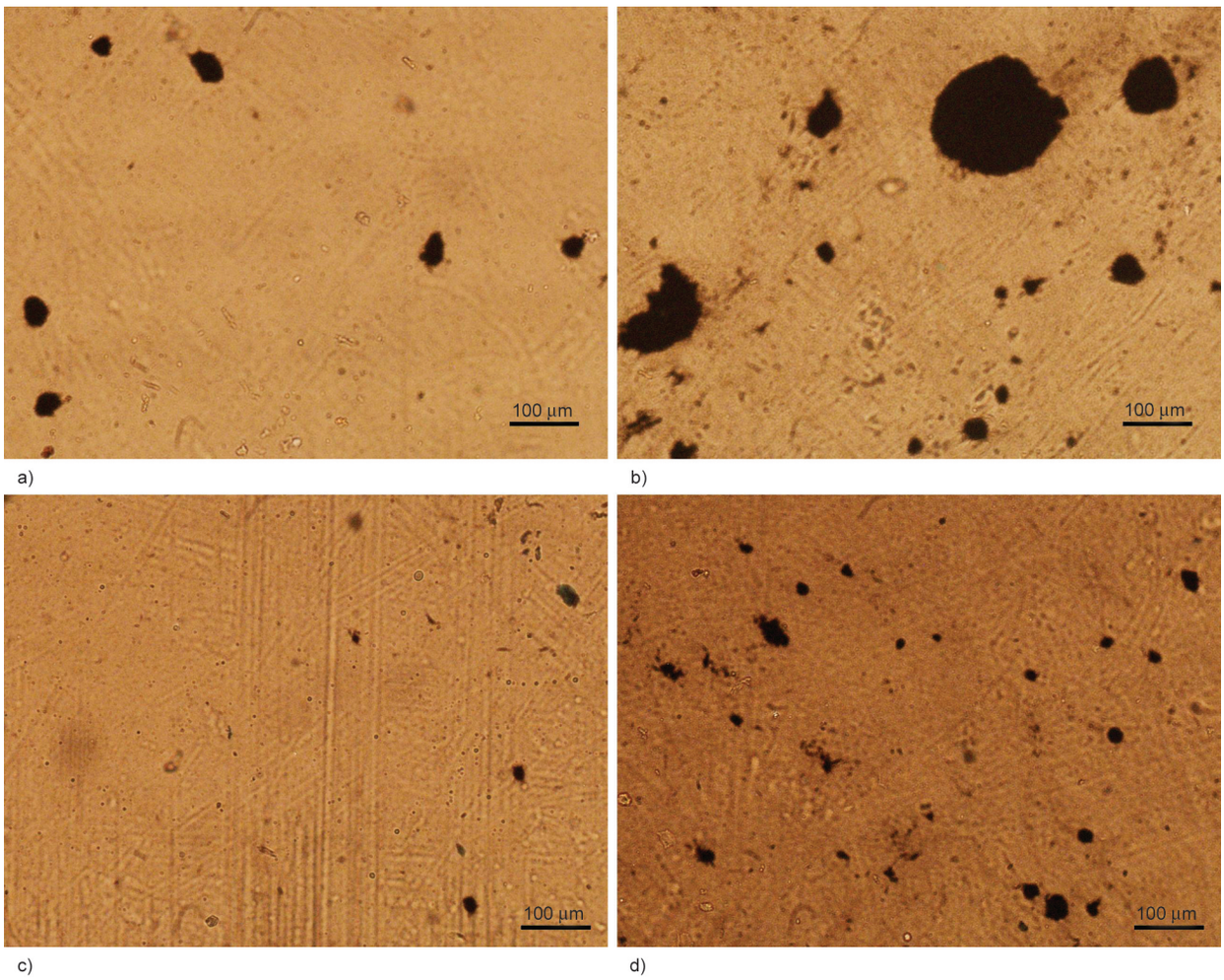

Figure 1. Morphologies of thin films of composites: a) PLAi 0.1, b) PLAi 1.0, c) PLAd 0.1, d) PLAd 1.0.

composite, which become visible when analyzing a representative volume of the examined sample. Such information is provided by light microscopy in the transmission mode through a thin layer of the composite. Figure 1 shows typical photographs of the tested composites. Dark inclusions are agglomerates of carbon nanotubes. As expected, agglomerates of micrometer sizes were present in limited numbers, depending on the concentration of filler and type of matrix.

The largest agglomerates were visible in the photographs of the PLAi 1.0 composite, the smallest in the case of the PLAd 0.1 composite. Intermediate, similar sizes of inclusions were visible for PLAi 0.1 and PLAd 1.0 composites. The agglomerates visible in the pictures have been measured, and histograms have been prepared to show the frequency of occurrence of agglomerates of certain sizes. These histograms are shown in Figure 2. They cover the size range from 3 to 150 µm. The histograms confirm the observations that the reduction of macromolecular entanglements has a positive effect on the distribution of carbon nanotubes inside the polymer. For example, in the PLAd 0.1 composite, almost 70% of the agglomerates had a size below 10 µm, while in the entangled PLAi 0.1 composite, the largest number of inclusions were 10–20 µm in size, and the size distribution was also much wider. An increase in filler content from 0.1 to 1.0 wt% increases the tendency to agglomerate. The number of large agglomerates with sizes above 50 µm is increasing. However, when comparing the PLAi 1.0 and PLAd 1.0 composites, it is clear that also, with higher nanotube contents, the reduction of macromolecular entanglements has a positive effect on their dispersion. Only single agglomerates larger than 50 µm were visible in the images for PLAd 1.0. It should be remembered that light microscopy images do not show inclusions below 3 micrometers, while SEM images (discussed later) showing such inclusions cover very small areas of samples and are of little use for calculating the proportion of inclusions of various sizes.

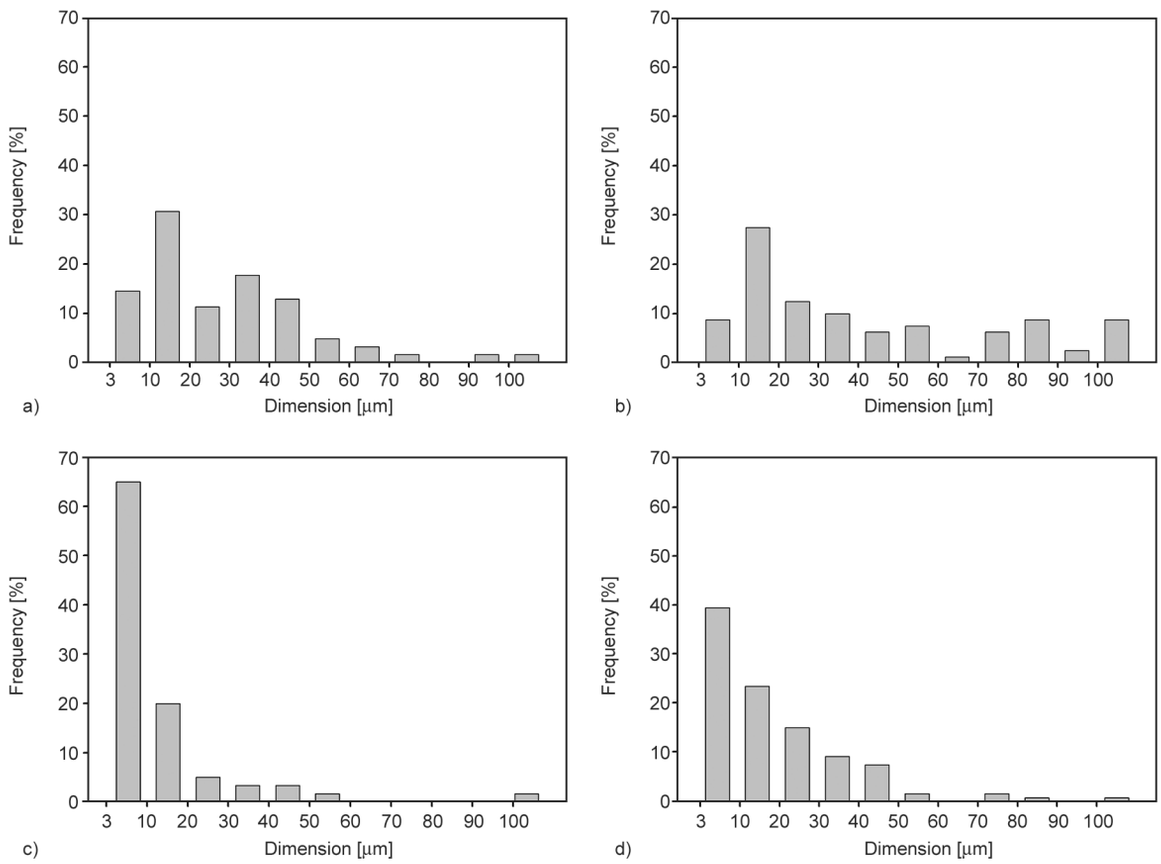

Figure 2. Histograms showing the frequency of occurrence of CNT agglomerates of various diameters: a) PLAi 0.1, b) PLAi 1.0, c) PLAd 0.1, d) PLAd 1.0.

It can be assumed that most of the MWCNTs used are finely dispersed and invisible in microscopic images. Although it is difficult to measure the contribution of the smallest particles to the total filler content, it can be roughly estimated from microscopic photographs. The ratio of the volume occupied by visible MWCNTs agglomerates, V_{CNT}, to the volume of the PLA, V_{PLA}, determined from photographs was: 0.78% for PLAi 0.1, 5.90% for PLAi 1.0, 0.38% for PLAd 0.1 and 1.84% for PLAd 1.0, respectively (see Table 2).

The ratio of the mass of visible MWCNTs, m_{CNT}, to the mass of PLA, m_{PLA}, may be calculated from the Equation (2):

$$\frac{m_{CNT}}{m_{PLA}} = \frac{V_{CNT}}{V_{PLA}} \cdot \frac{\rho_{CNT}}{\rho_{PLA}} \tag{2}$$

where ρ_{CNT} is the density of MWCNTs filler, and ρ_{PLA} is the density of PLA. According to the manufacturers, the bulk density of MWCNTs is equal to 0.075 g/cm^3, and the density of PLA is equal to 1.24 g/cm^3. During melt processing, mobile macromolecules penetrate the free space between the nanoparticles, applying moderate pressure on the nanotube assemblies. If we assume that there was no significant compression of nanotubes, the density of MWCNTs inside the polymer should be close to the bulk density of MWCNTs. According to this

Table 2. Volume (V_{CNT}/V_{PLA}) and mass (m_{CNT}/m_{PLA}) ratios of MWCNTs and PLA determined by optical microscopy (OM) and calculated fractions of MWCNTs invisible in the microscope.

Composite	V_{CNT}/V_{PLA} [%]	m_{CNT}/m_{PLA} [%]	Mass content of CNTs inserted into composite [%]	Mass content of nanoparticles not visible by OM [%]
PLAi 0.1	0.78	0.05	0.1	50
PLAi 1.0	5.90	0.35	1.0	65
PLAd 0.1	0.38	0.02	0.1	80
PLAd 1.0	1.84	0.11	1.0	89

assumption, it can be calculated from Equation (2) that the m_{CNT}/m_{PLA} ratios in examined composites were 0.05% for PLAi 0.1, 0.35% for PLAi 1.0, 0.02% for PLAd 0.1 and 0.11% for PLAd 1.0. Comparison of these values with the fact that the total content of MWCNTs in the composites was 0.1 or 1.0% means that most of the MWCNTs were dispersed to such an extent that they were not visible in the light microscope. The last column in Table 2 shows what percentage of the nanofiller was below 3 μm. For all composites, at least 50% of the nanotubes were dispersed at the nano level, *i.e.*, good dispersion was obtained. Comparing the composites with the same filler content but with less or more entangled macromolecules, it can be seen that better dispersion of the filler occurs in the partially disentangled PLA composite.

The morphologies of the composites at higher magnifications, available in scanning electron microscopy, were also observed. The photographs in Figure 3. show that more agglomerates were present in composites with entangled macromolecules, especially when the filler content increased from 0.1 to 1 wt%. For example, single agglomerates with a diameter of 3–5 μm are visible in Figure 3b, while in the PLAd matrix (Figure 3d), the size of the agglomerates does not exceed 2 μm. When only 0.1 wt% of MWCNTs was introduced into the matrix, smaller agglomerates can be seen in the photographs (Figure 3a), and in the PLAd 0.1 composite, they are even poorly visible (Figure 3c). As can be seen from the calculations in Table 2 and from the SEM observations, although there are agglomerates in the composites, most of the CNTs are dispersed at the nanometer level.

3.2. Non-isothermal crystallization

Non-isothermal crystallization was investigated by DSC. The typical heating-cooling-heating protocol was used. In the case of limiting the entanglement of macromolecules, a possible change in the value of the glass transition temperature (T_g) could be expected. In the published studies of PLA-MWCNTs composites, there were conflicting reports about the

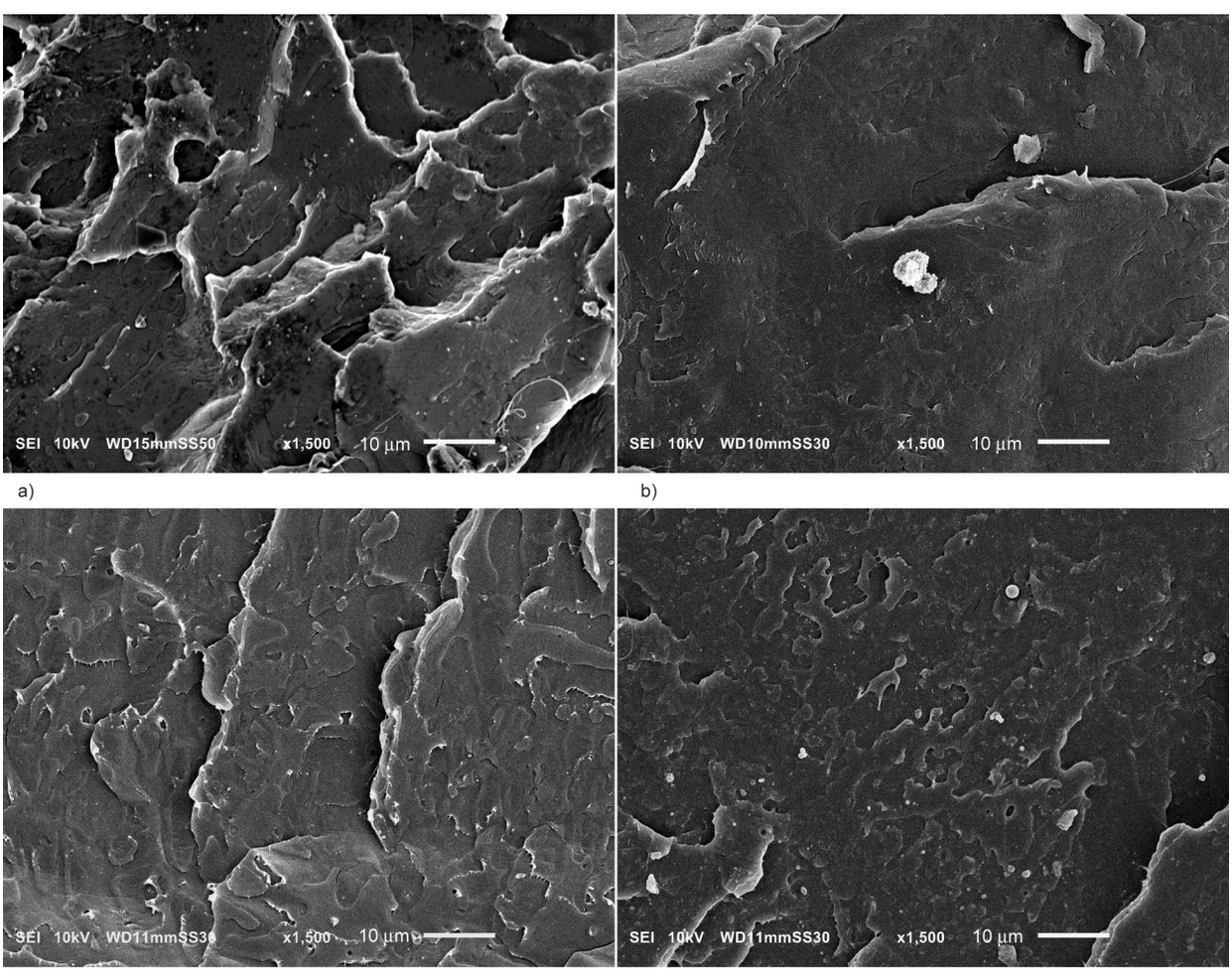

Figure 3. Morphology of the internal surface of composite: a) PLAi 0.1, b) PLAi 1.0, c) PLAd 0.1, d) PLAd 1.0.

Table 3. Glass transition temperatures measured in DSC non-isothermal experiment.

Sample	I. Heating [°C]	Cooling [°C]	II. Heating [°C]
PLAi	57.4	58.9	60.7
PLAi 0.1	54.6	59.5	62.1
PLAi 1.0	55.3	58.2	62.4
PLAd	57.1	58.8	62.1
PLAd 0.1	55.6	60.8	61.6
PLAd 1.0	56.6	61.0	62.2

change or no change in the glass transition in the presence of filler [10, 11]. Therefore, when analyzing the results of DSC, we first focused on the glass transition temperature. The results of T_g measurements are presented in Table 3. The determined glass transition temperatures depended somewhat on the phase of the temperature cycle in which they were measured. However, changes in T_g related to the disentangling of macromolecules or the presence of nanotubes were not systematic and were within the range of accuracy of temperature determination.

Table 4 presents the thermal transitions that were observed in non-isothermal DSC studies above the glass transition. When calculating the degree of crystallinity, it was taken into account that the heat of melting of 100% crystalline PLA is 93 J/g [41, 42] and that the mass fraction of PLA in the composites is less than 100%. The first heating reflects the state of the material created during its preparation. When the temperature of the sample increased to 98.4–105.1 °C, depending on the material, cold crystallization, *i.e.*, solid-state crystallization, was observed. Changes in the cold crystallization temperature (maximum of peak) were not large and it was difficult to see regularity related to the composition of the sample or degree of entanglement of macromolecules.

The measured heat of cold crystallization was high, and the calculated increase in crystallinity was 32–44%. Considering that for PLA, it is difficult to achieve crystallinity above 40% [43], this means that before the measurements, the tested composites had a low content of the crystalline phase. The crystallinity obtained by cold crystallization (X_{cc}) was lower for PLAd than for PLAi and regularly decreased with the content of nanotubes in the composite. The difference between the polylactides is probably due to the different polymer preparation procedures and the smaller amount of nuclei present in PLAd. On the other hand, the reduction of cold crystallization with the increase in the content of MWCNTs indicates their barrier role for this type of crystallization.

In all tested samples, with the exception of PLAd, a slight exothermic transformation was visible at 155–156 °C with the heat of 0.2–1.5 J/g. This transformation, just prior to the melting of the material, is attributed to the transformation of the α′ crystalline phase in PLA into the more stable α phase [44].

The melting process observed during the first heating reached its maximum at the temperature of 166.9–169.4 °C without a regular dependence on the composition of samples. The total crystallinity (X_m) determined from the heat of melting showed a similar tendency as the crystallinity of cold crystallization. It was higher for PLAi than for PLAd and regularly decreased with the addition of nanotubes. The difference between the X_m and X_{cc} values, characterizing the initial crystallinity and amounting to 1.3–5.7%,

Table 4. The results of non-isothermal crystallization experiment.

Sample	I. Heating				Cooling		II. Heating			
	T_{cc} [°C]	X_{cc} [%]	T_m [°C]	X_m [%]	T_c [°C]	X_c [%]	T_{cc} [°C]	X_{cc} [%]	T_m [°C]	X_m [%]
PLAi	99.5	43.5	166.9	48.3	93.1	5.9	100.4	34.7	166.8	45.8
PLAi 0.1	105.1	39.4	169.5	40.7	89.6	3.1	102.4	33.1	168.2	40.2
PLAi 1.0	102.2	34.6	168.9	40.3	89.4	4.7	99.1	28.3	168.3	38.2
PLAd	105.3	40.2	169.4	42.0	94.1	0.7	125.1	37.5	168.8	42.5
PLAd 0.1	100.3	36.1	168.4	40.4	98.5	23.1	96.6	9.8	167.9	40.5
PLAd 1.0	98.4	31.7	168.9	36.1	100.5	27.6	105.7	3.8	168.5	38.7

T_{cc} – cold crystallization temperature,
T_m – melting temperature,
T_c – crystallization temperature,
X_{cc} – crystallinity calculated from the heat of cold crystallization,
X_m – total crystallinity determined from the heat of melting,
X_c – crystallinity calculated from the heat of crystallization on cooling.

confirmed that the crystallinity of the samples before the DSC tests was low.

The interesting effects were observed when cooling the melt, during which crystallization of polylactide happened. Crystallization of PLAi and PLAi 0.1, PLAi 1.0 composites started at temperatures of 111–113 °C. The temperature of the beginning of crystallization in PLAd was similar, although it was difficult to determine it precisely due to the weakness of the effect. The temperatures of the beginning of crystallization in the PLAd 0.1 and PLAd 1.0 composites were much higher, at 122.4 and 121.1 °C, respectively. The maximum (peak) crystallization temperature was similar for both homopolymers, one degree higher for PLAd. However, as the filler content increased, the temperature representing the maximum changed differently for the entangled and disentangled PLA matrix composites. In the fully entangled PLAi composites, the maximum crystallization was shifted to lower temperatures after the addition of carbon nanotubes. It can be assumed that the presence of nanotubes limits the movement of macromolecules to growing crystals, not compensated by additional nucleation on MWCNTs. The crystallinity in PLAi and its composites is low (3–6%), and it decreases in the composite, which supports the assumption that nanotubes are more crystallization obstacles than promoters as crystallization nuclei.

Crystallization in PLAd composites proceeded differently. The PLAd homopolymer obtained very low crystallinity on cooling, but the PLAd 0.1 and PLAd 1.0 composites crystallized easily. After adding MWCNTs to PLAd, the maximum crystallization temperature (from 94.1 to 100.5 °C) and the degree of crystallinity (from 0.7 to 27.6%) significantly increased. Better dispersion of the filler in PLAd composites than in PLAi composites meant that a larger fraction of nanoparticles present in the polymer could cause nucleation of crystallization. With the greater mobility of the less entangled macromolecules, the combined effect of enhanced nucleation and easier transport outweighed the fact that the nanotubes were obstacles to the movement of macromolecules to crystallization sites. As a result, a significant increase in the degree of crystallinity was observed during the cooling of composites with disentangled macromolecules.

The behavior of materials observed during the second heating depended on the previous crystallization during cooling. The well-crystallizing PLAd 0.1 and PLAd 1.0 composites showed limited cold crystallization. PLAi, PLAd, PLAi 0.1, and PLAi 1.0, which crystallized poorly on cooling, showed effective cold crystallization. For PLAi composites, a certain reduction in the degree of crystallinity was visible with an increase in the CNT content. PLAi and PLAi composites began to cold crystallize at 81–83 °C, similarly to PLAd 0.1 (81.1 °C), while the cold crystallization in PLAd 1.0 started at 88.0 °C. The maximum of the cold crystallization peak was observed at the temperature of 96.6–105.7 °C. Considerably delayed, probably due to the limited number of nuclei, was the crystallization in PLAd. Its beginning was at 93.5 °C, maximum at 125 °C, and the crystallization peak smoothly turned into a melting peak.

During the second heating, in most materials, with the exception of PLAd and PLAd 1.0, there was a slight α′-α transition peak, visible at 153.5–154.6 °C, with the heat of transition of 1.1–3.1 J/g. At temperatures above 154 °C, the melting process began to be visible. The melting temperatures during the second heating were similar for all studied materials (166.8–168.8 °C). The total crystallinity of PLAi and PLAd composites was in the range of 38.7–45.8% and slightly decreased with the increase in the content of nanotubes. The measured total crystallinity resulted from previous normal and cold crystallization.

3.3. Isothermal crystallization

The crystallization properties of polymers and composites were also examined in isothermal conditions. Based on the results in non-isothermal conditions, knowing the temperatures of the beginning of crystallization during cooling, two temperatures were selected for isothermal tests: 120 and 125 °C. The time dependencies of the heat flow are shown in Figure 4, and the characteristic times of crystallization are shown in Table 5. In all examined materials, crystallization at 120 °C proceeded faster than at 125 °C. The dynamics of isothermal crystallization depend on two factors: nucleation and rate of crystal growth. We previously determined the lamella growth rate for this polymer, which was 2.15 μm/min at 120 °C and 2.25 μm/min at 125 °C for PLAi and 2.25 μm/min at 120 °C and 2.35 μm/min at 125 °C for PLAd [31]. Nucleation was not determined in these studies, but it is usually more intense in semi-crystalline polymers at lower crystallization temperatures. As a result of the interaction of both factors, it takes much longer to crystallize at 125 °C.

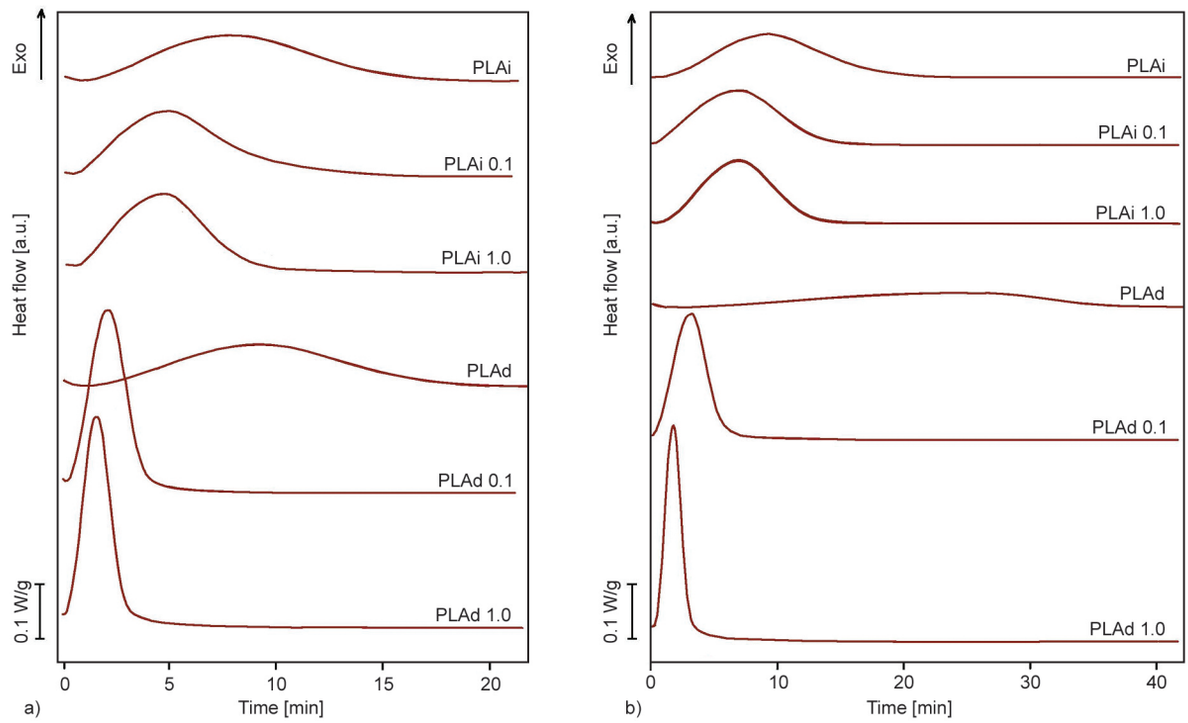

Figure 4. Changes of heat flow with time recorded during isothermal crystallization at 120 °C (a) and 125 °C (b).

Table 5. Times characterizing isothermal crystallization at 120 and 125 °C and heat of crystallization.

Material	T = 120 °C				T = 125 °C			
	t_{min} [min]	t_{max} [min]	t_{end} [min]	Heat [J/g]	t_{min} [min]	t_{max} [min]	t_{end} [min]	Heat [J/g]
PLAi	1.0	7.9	19.0	38	1.0	10.0	21.9	43
PLAi 0.1	0.7	5.0	15.9	40	0.3	8.1	20.0	43
PLAi 1.0	0.7	4.7	13.5	37	0.5	7.5	18.3	42
PLAd	1.3	9.2	21.0	40	1.6	24.0	39.0	43
PLAd 0.1	0.3	2.0	9.7	37	0.3	4.1	16.3	40
PLAd 1.0	0.0	1.6	8.5	37	0.3	3.0	14.5	41

t_{min} – start time of crystallization,
t_{max} – time when the maximum heat flow was observed,
t_{end} – end time of crystallization.

Comparing both homopolymers, *i.e.* PLAi and PLAd, the second one needed more time to crystallize. As discussed during the non-isothermal crystallization, some nuclei were removed from the PLAd during solvent treatment. The greater difference in crystallization time of both homopolymers observed at 125 °C, when the activity of the present nuclei decreases, confirms that there were fewer nuclei in PLAd. The slightly faster crystal growth rate in PLAd did not compensate for the lower nucleation.

For composites, the addition of nanotubes shortened the crystallization time. However, significantly more MWCNTs particles in 1.0 wt% of composites give only a slight shortening of crystallization compared to 0.1 wt% composites. Increasing the content of nanotubes provides additional nuclei, but only some of the nanotubes nucleate polylactide. On the other hand, almost all nanoparticles are an obstacle to the movement and crystallization of polymer chains and there are definitely more of them in the composite with 1.0 wt% MWCNTs by weight. Therefore, the crystallization time is only slightly shortened with the increase in the content of nanotubes.

Table 5 also shows that the crystallization process was faster in composites with partially disentangled chains than in their fully entangled counterparts. Better dispersion of MWCNTs, providing more active nuclei, and greater mobility of macromolecules are

the reasons for this faster crystallization, although improved dispersion also means more obstacles from nanotubes in the path of macromolecules.

The heat of crystallization for each material was higher at a temperature of 125 °C than at 120 °C because the total time of process was longer, and some annealing just formed crystals increased the total crystallinity. The heats of crystallization of composites were slightly lower than for homopolymers; however, the observed changes were not regular.

3.4. Thermogravimetry

In order to determine whether a less entangled matrix or the presence of nanotubes affects the thermal stability of the tested materials, thermogravimetric measurements were performed. The change in the mass of the tested sample as a function of temperature and the derivative of the change in this mass are shown in Figure 5. Thermal degradation of all samples occurred in the same temperature range of 270–400 °C. The dynamics of the process were very similar for both PLAs and their composites. The temperature at which the mass of the sample changed the fastest was slightly higher in the composites. It was 367 °C for PLAi and 369 °C for PLAi 1.0. In the case of partially disentangled materials, this temperature was 365 °C for PLAd and 368 °C for PLAd 1.0.

The slight decrease in temperature observed for the partially disentangled polymer can be attributed to easier access to the polymer volume. On the other hand, a slight increase in the temperature of the fastest degradation in composites is caused by the barrier effect resulting from the presence of fillers. Although a slight influence of the structure of the samples on the thermal resistance is visible, it generally does not affect the good stability of the materials.

3.5. Mechanical properties

The conditions for mechanical testing were first established using PLAi samples subjected to tensile tests at different temperatures. The strain-stress curves of PLAi are shown in Figure 6a. It can be seen how quickly the yield stress decreases with increasing temperature. This stress was 73 MPa at 20 °C, 49 MPa at 40 °C, and 32 MPa at 50 °C. At a temperature of 20 °C, which is well below the glass transition, the possibilities of movement of 'frozen' PLA macromolecules were very limited, which led to the rapid breaking of the samples. From theoretical considerations, it is known that the influence of the degree of entanglement of the macromolecular network on the properties should be visible primarily at higher strains, where strain hardening occurs. Therefore, the tests of partially disentangled samples should be carried out at a temperature where large deformations are possible. As seen in Figure 6a, the deformability of PLAi significantly increases at higher temperatures.

Disentanglement of the polymer usually increases the probability of brittle failure due to the easier formation of voids inside the material, but this negative effect decreases with increasing temperature as the mobility of macromolecules increases. For the above reasons, it would not be a good idea to test our polymers and composites at ambient temperature, but good testing conditions could be expected above the glass transition temperature.

Observations of the samples during and after the test showed that the mechanism of deformation changed

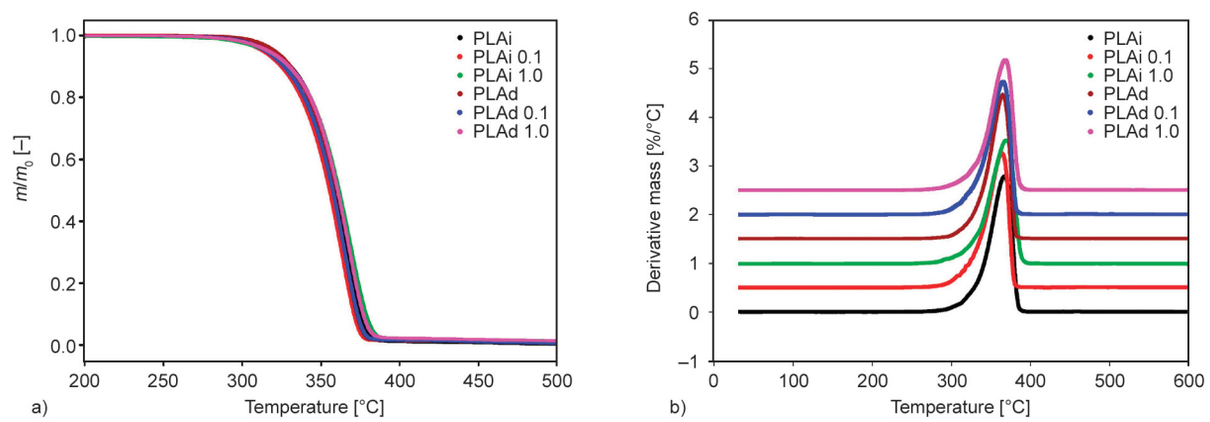

Figure 5. a) The ratio of the current, m, and initial mass of the sample, m_0, as a function of temperature during heating in nitrogen atmosphere; b) derivative of mass loss during heating. The black curve in Figure 5b is in its original positions, the other curves have been proportionally (0.5 each) shifted vertically for better visibility.

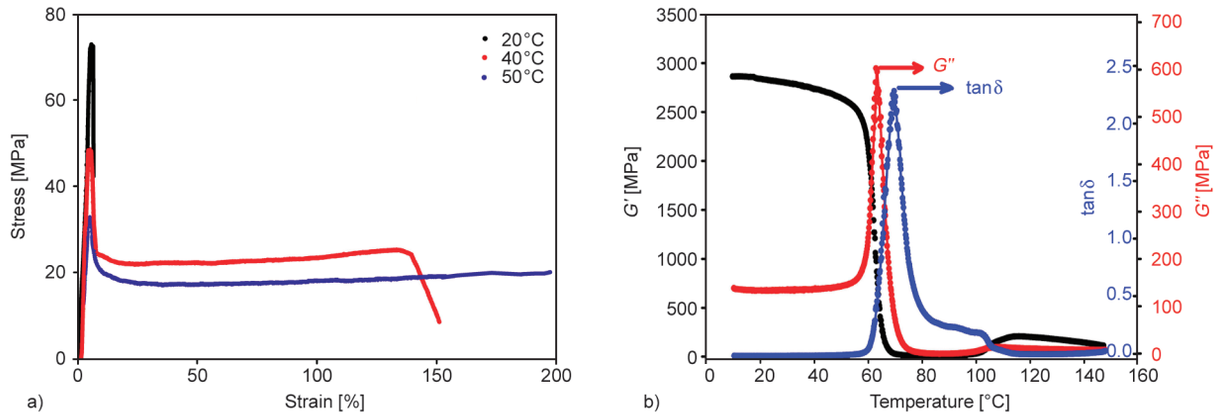

Figure 6. a) Mechanical properties of PLAi determined during tensile test at temperatures of 20, 40 and 50 °C; b) storage modulus (G'), loss modulus (G'') and tan δ measured for PLAi samples at temperatures of 10–160 °C.

as a function of temperature. It was a brittle fracture with signs of crazing before the break when tested at 20 °C, formation of a localized single shear band with necking at 40 °C and almost uniform deformation at 50 °C.

To determine the best temperature for tensile testing of our PLA, the DMTA, studies were conducted (Figure 6b). Experiments have shown that the glass transition occurs at a temperature range of 50 to 70 °C. The maximum of G'' was observed at 62.5 °C, and the maximum of tan δ was at 68.7 °C. The storage modulus remained constant from 70 °C. For these reasons, the tensile properties of our samples were examined at 70 °C, where a large deformation could be observed, including the strain-hardening phase. Similarly, other authors interested in PLA deformation mechanisms conducted research at temperatures of 70 °C and higher [2, 44].

The results of the tensile test of PLAs and composites at 70 °C are shown in Figure 7. The exemplary strain-stress curves are shown. All tested materials were able to achieve high engineering strains of 350–500%. The yield point was reached at 50–55% strain for homopolymers, increasing to the strain of 65–70% for composites. However, no strong localization of deformation at the yield was observed in the form of a neck appearing in the tested sample. The yield stress values are shown in Table 6. As expected, the stress values at high test temperatures were low, less than 1 MPa. At the yield point, it is seen that less stress is needed to initiate the plastic deformation in the less entangled PLAd polylactide. For both polymers, the yield strength increased with the content of nanotubes, indicating some reinforcement of the matrix by MWCNTs, which is more effective in PLAd composites. The standard deviations for the tested samples were 4–8% of mean values (Table 6), which proves good repeatability of measurements.

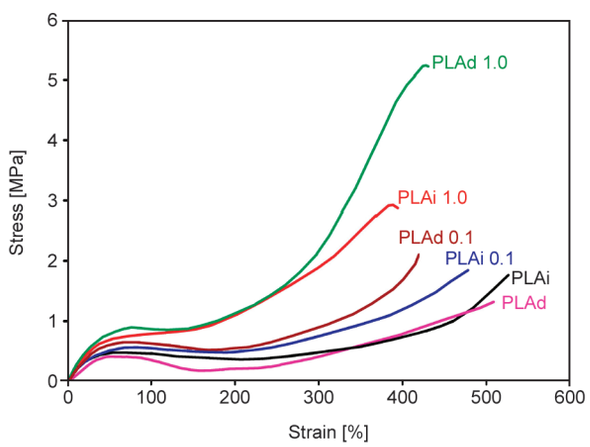

Figure 7. Representative strain-stress curves showing the mechanical properties of the samples in a tensile test at 70 °C.

At elongations beyond the yield point, the deformed sample entered the plateau stage, in which no significant changes in stress are usually observed. In the tested samples, this phase was relatively short and ended at a strain of about 150%.

Significant differences between the studied materials appeared at large deformations. After a short drop and a plateau in the curves, the next stage of deformation, called strain-hardening, began (at the strain

Table 6. Yield stress (σ_y) measured at 70 °C.

Sample	σ_y [MPa]
PLAi	0.51±0.02
PLAi 0.1	0.55±0.04
PLAi 1.0	0.67±0.03
PLAd	0.48±0.02
PLAd 0.1	0.63±0.03
PLAd 1.0	0.84±0.03

of 200–250%). During strain-hardening, the stress measured in the tested samples increased quickly, and there were significant differences between the samples. One of the factors responsible for the rate of stress increase is the density of macromolecular entanglements, which determines the stronger or softer reaction of the deformed macromolecular network in the polymer. This is the reason for the slow increase in stress for partially entangled PLAd and greater for fully entangled PLAi. The second factor influencing the course of strain-hardening is the presence of nanofillers in the composites. In the case of both polylactide matrices, the increasing amount of dispersed filler accelerated the stress increase and shifted the beginning of the hardening phase to smaller strains. With the same content of nanotubes, a stronger reinforcement effect was seen in the composite with a less entangled amorphous phase. For example, in the PLAd 1.0 composite, at 350% strain, the stresses were 1.4 times higher than in the PLAi 1.0 composite (3.4 *vs*. 2.5 MPa) and 5 times higher than in the PLAd polymer. The differences between the composites can be attributed to the previously discussed better dispersion of the filler. Thus, well-dispersed, numerous nanotubes have a stronger effect on the strain-hardening than the reduction of entanglements in the PLA macromolecules network.

In order to learn more about the changes taking place inside the composites during deformation, measurements of their shape (*i.e.*, length, width, and thickness) in the function of time were made. Knowing the changes in shape, it was possible to calculate the change in volume in a selected fragment of the sample. Such measurements are usually made for the first deforming part of the sample, where structural changes during plastic deformation occur fastest. However, in the case of the tested materials, the deformation of individual parts of the sample occurred similarly, so the selection of the right fragment was less important. Figure 8a shows how the width W and thickness D of the samples decreased during deformation in the example of the PLAd sample. Size changes were very similar for the other materials tested (not shown here). In the applied experimental

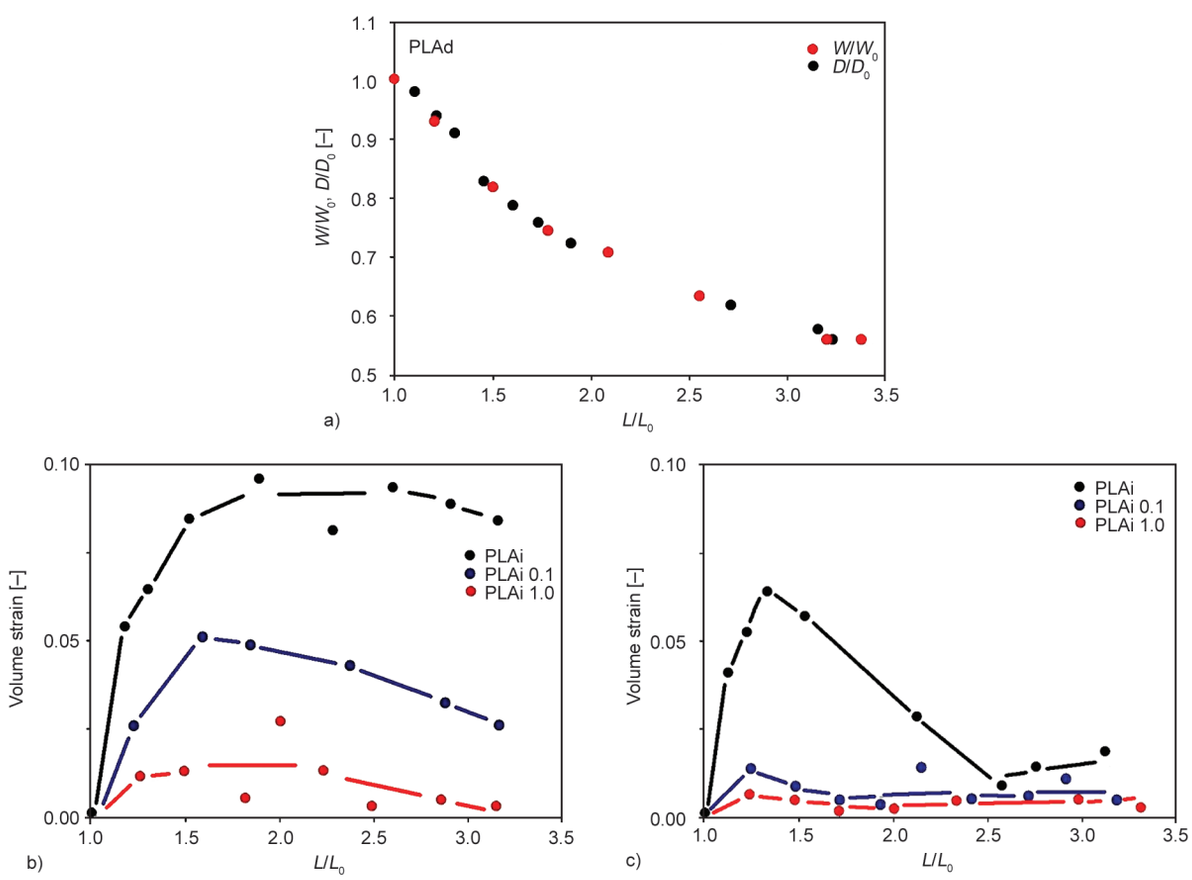

Figure 8. a) Changes in the dimensions of the sample during deformation measured for PLAd. L – actual length, L_0 – initial length, W – actual width, W_0 – initial width, D – actual thickness, D_0 – initial thickness; b) volume strain calculated for PLAi and its composites; c) volume strain calculated for PLAd and its composites. The lines connecting the points are intended to help the reader notice the trends of the results.

conditions, changes in thickness were very similar to changes in the width of the tested sample, which means that the shape of its cross-section did not change.

Figure 8b and Figure 8c show volume changes during the deformation of the tested materials, calculated according to Equation (1). The increase in volume in our polylactides was relatively low. The largest increase in volume was observed for PLAi (0.10 at L/L_0 = 2.0) and PLAd (0.07 at L/L_0 = 1.4). In the composites, with the increase of the MWCNTs content, the volume strain decreased to almost zero. This decrease was faster when the matrix was less entangled, most likely as a result of better nanoparticle dispersion. The very small volume strain of the composites supported the assumption that limited micro cavitation was present only in PLAi and PLAd. The scale of cavitation, and thus the increase in volume, depends on the possibility of relaxation of local stresses in the matrix. Both the greater mobility of less entangled macromolecules and the better MWCNTs dispersion prevent stronger stress concentration in the PLA matrix.

Analyzing the volume strain with the progress of deformation, it can be seen that the volume rapidly increased until the local deformation of 1.5–2.0. Since the samples deformed almost uniformly, this corresponded to engineering strain of 50–100%, *i.e.*, deformation just after yielding (see Figure 7), when the structure of the polymer is reorganized, and cavities usually are initiated. For larger strains (*i.e.*, for L/L_0 = 2.5–3.0), a decrease in the volume strain is observed, usually explained by a change in the shape of the voids into more elongated but thinner, and therefore with a smaller volume of each void.

In order to better understand the structural changes that occurred in the tested materials, the samples after the tensile test were characterized by X-ray methods, and WAXS and SAXS tests were performed. X-ray experiments were conducted to clarify three issues: the occurrence of crystallization due to deformation, the orientation of structural elements, and the appearance of nanocavitation. The answer to the first question can be provided by the WAXS 2D experiment; the nanovoiding and orientation of the nanotubes should be visible in the SAXS patterns.

WAXS 2D scattering images from the tested samples before and after deformation up to 350% of strain are shown in Figure 9. For non-deformed homopolymers and composites, only scattering in the amorphous phase is visible, which confirms the absence of a crystalline phase and agrees with the previously discussed results of DSC studies on crystallization. The scattering images changed after the samples were deformed. In the case of both polylactides, a strong localization of signals is visible and the patterns resemble those observed for fibers. The scattering is mainly from the newly formed crystalline phase, although a weakened amorphous hallo is still visible. The ring fragments (arcs or blobs) represent

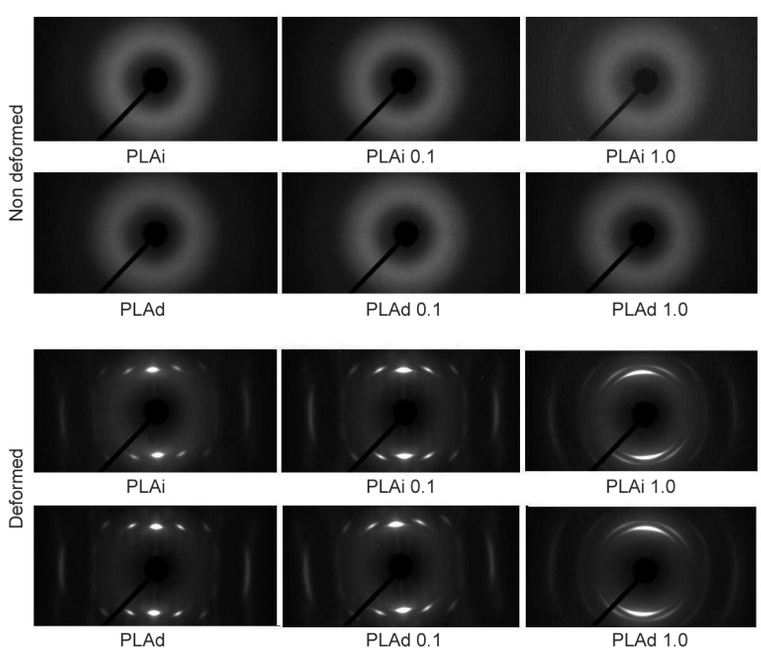

Figure 9. WAXS patterns registered for non-deformed samples and samples deformed to strain of 350%. The direction of stretching in the photographs was horizontal.

the scattering at 2θ angles of 16.7°, 19.1°, 24.9°, and 33.0°. The last two reflections are hardly visible. The most intensive reflection (*i.e.*16.7°) is visible in the vertical direction, and the last one (33.0°) is in the horizontal direction, *i.e.*, in the direction of stretching. The reflection at 2θ =16.4° is assigned to the (200) and (110) crystal planes and the reflection at 2θ = 18.7° represents the diffraction on the (203) crystal plane [3, 43]. The lack of reflections at 2θ = 14.8° and 22.2° indicates that the less ordered α′ form rather than the α form was formed in the sample [2]. The location of reflections (200) and (110) indicates a strong orientation of the macromolecules forming crystals in the direction of deformation.

A very similar evolution of polylactide WAXS patterns was observed with the progress of deformation by Stoclet *et al*. [2] and Zhang *et al*. [45]. They noticed that patterns indicating crystallization in the sample were first seen shortly before or at the beginning of the strain-hardening phase. Stoclet *et al*. [2] have seen much weaker crystalline scattering at 70 °C than is visible in Figure 9; however, it may be explained much faster deformation rate in their case, limiting the time available to crystallization during the experiment. On the other hand, Zhang *et al*. [45] observed that an increase in strain rate tends to favor crystallization. In Zhang's work, it was also shown that annealing for the time corresponding to the tensile experiment did not lead to the formation of a crystalline phase. This agrees with our supplementary observations. Thus, the patterns of PLAs in Figure 9 are the result of strain-induced crystallization, not annealing during deformation.

Scattering images after deformation for PLAi 0.1 and PLAd 0.1 composites are very similar to those recorded for polylactide. A thorough analysis, however, shows slightly less concentration of reflections, *e.g.*, from the (200)/(110) planes. The change in the shape of the reflections, which take the form of arcs, increases with the content of MWCNTs in the composites. This can be clearly seen in the scattering images on PLAd 1.0 and PLAi 1.0 composites. The presence of nanotubes makes it difficult to orientate macromolecules and the resulting crystals are therefore less oriented with the increase in the content of the nanofiller.

It required clarification on whether the composition of the material affected the intensity of crystallization caused by deformation and whether, for example, crystals of different thicknesses grew. Information on these topics was provided by DSC studies of deformed samples, carried out by heating to the melt state. The measurement results are presented in Table 7. Compared to the data in Table 3, an increase in the glass transition temperature of about 2 °C is noticeable.

The tested materials, apart from PLAd 1.0, showed limited cold crystallization, occurring at temperatures 15–20 °C lower than the temperatures measured previously for non-oriented samples (see Table 4). Melting took place at temperatures of 165.8–166.4 °C, and their small dispersion indicates a similar thickness of crystals present in different samples. Differences between the heat of melting and the heat of cold crystallization show the crystallinity of the deformed samples. The degree of crystallinity determined after deformation was at the level of 40–45%, similar for all tested materials.

Figure 10a shows small-angle scattering images recorded for non-deformed samples. There is a visible lack of orientation and an increase in the intensity of scattering with the increase in the content of

Table 7. Temperatures and heats of crystallization and melting measured for samples stretched to 350% strain.

Sample	T_g [°C]	T_{cc} [°C]	H_{cc} [J/g]	T_m [°C]	H_m [J/g]	$H_m - H_{cc}$ [J/g]	X [%]
PLAi	60.2	79.1	9.8	166.1	47.5	37.7	40.5
PLAi 0.1	60.1	88.9	2.7	165.8	44.5	41.8	44.9
PLAi 1.0	59.6	88.9	2.7	166.4	42.0	39.3	42.3
PLAd	65.8	89.0	2.7	165.8	43.1	40.4	43.4
PLAd 0.1	58.1	89.9	3.6	166.1	43.5	39.9	42.9
PLAd 1.0	57.3	–	–	166.2	42.0	42.0	45.2

T_g – glass transition temperature,
T_{cc} – cold crystallization temperature,
T_m – melting temperature,
H_{cc} – heat of cold crystallization,
H_m – heat of melting,
X – crystallinity of samples before the cold crystallization.

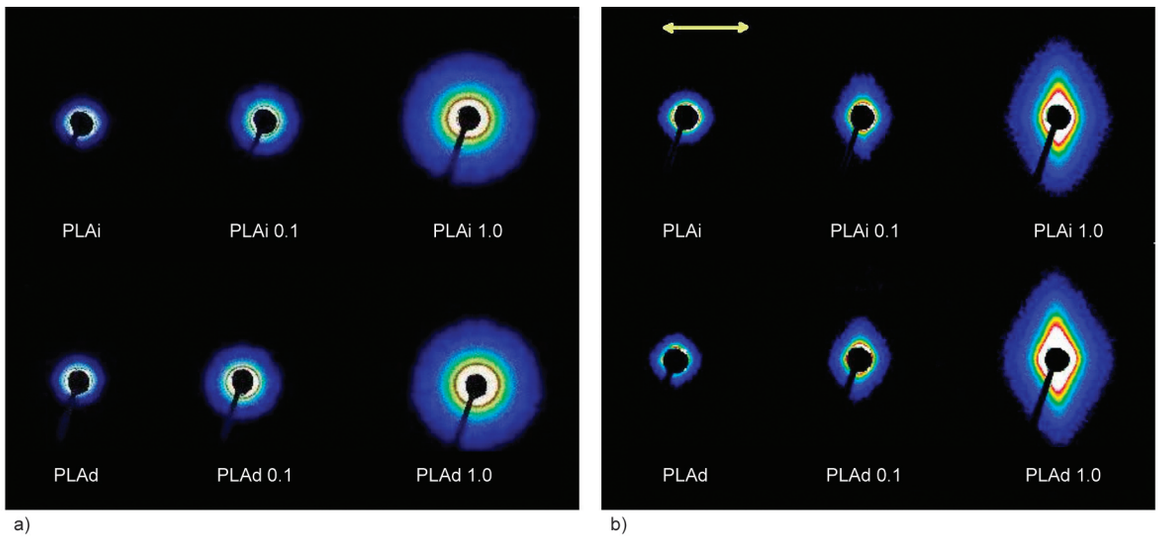

Figure 10. Small-angle X-ray scattering on the tested materials: a) non-oriented samples, b) samples after deformation in the tensile test up to 350%. The yellow arrow shows the direction of stretching.

MWCNTs in the composites. The scattering of X-ray on polylactide only comes from the amorphous phase and is, therefore weak. In composites, it is accompanied by intense scattering on nanotubes. Scattering images recorded for samples deformed to 350% of strain are shown in Figure 10b. Patterns for PLAi and PLAd have not changed significantly, and the orientation of the polymers is not visible on them. Also, the intensity of scattering was similar for homopolymers before and after deformation. The studied samples had the same thickness, so it was possible to compare intensity and scattering profiles. Profiles taken in the vertical direction in Figure 10 are shown in Figure 11a, and Figure 11b. Figure 11c

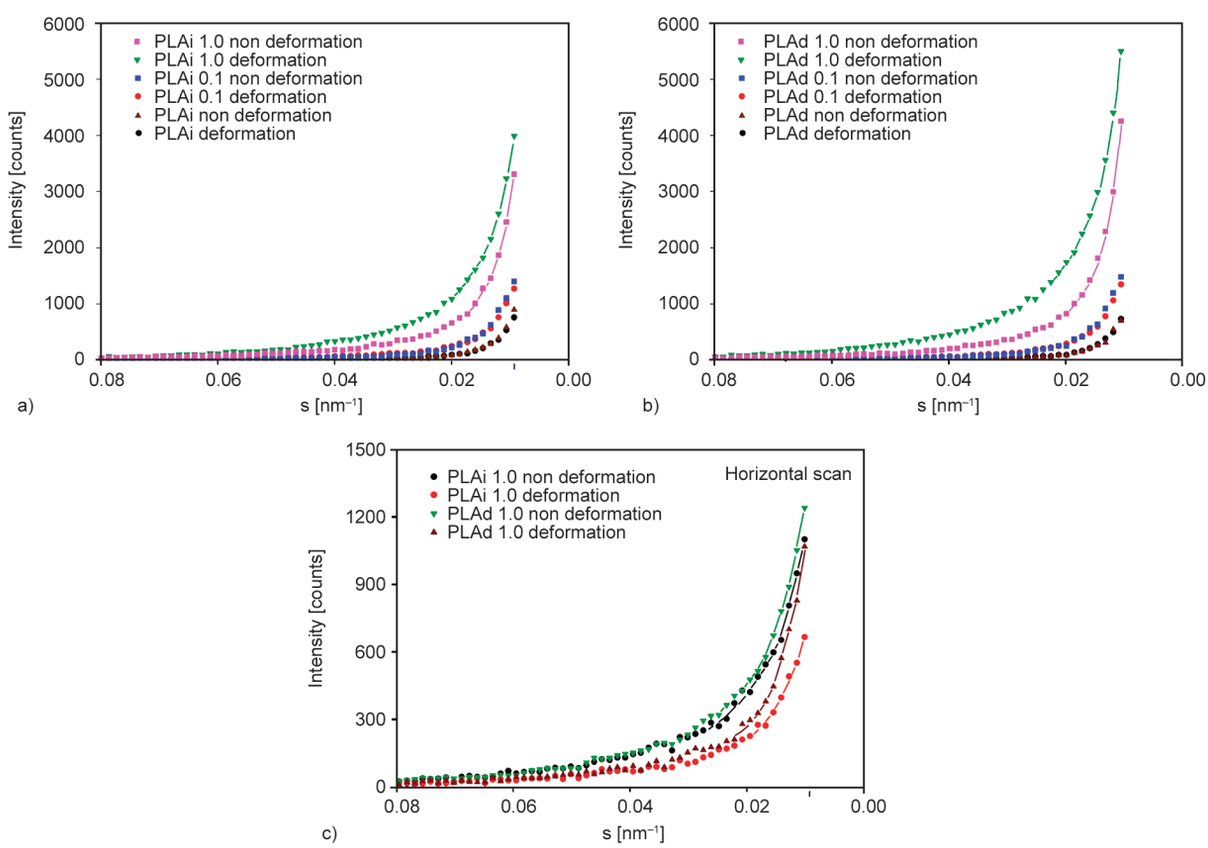

Figure 11. Scattering intensity profiles taken from the SAXS patterns in Figure 10 in the vertical PLAi (a), and PLAd (b) and horizontal (c) directions. On the horizontal axis is the wave vector, s.

shows profiles in the horizontal (stretching) direction for selected samples.

The important issue is whether there are changes in scattering that indicate crystallization or cavitation. From the results of WAXS studies, it was expected that the formation of the periodic crystal structure should be visible in the SAXS patterns, mainly in the horizontal direction. In the case of crystallization, parameters such as long period and lamella thickness can usually be specified based on SAXS. However, for deformed, semi-crystalline PLAi and PLAd samples, the additional scattering is small, which makes it very difficult to determine the above parameters. This is explained by the fact that the density of the amorphous phase is close to the density of the imperfect α′ crystalline phase, which makes the scattering intensity on the periodic structure low [44, 46]. Similarly to microvoids also nanovoids can be generated during polylactide deformation, which should be seen as a rapid increase in scattering intensity. Such additional scattering is not visible when comparing intensity profiles for deformed and non-deformed polylactides. This means that the formation of nanovoids did not occur in homopolymers. Zhang *et al*. [45] observed nanocavitation during the deformation of amorphous polylactide at a temperature of 75 °C, but this phenomenon occurred for higher strain rates, with large strains. The minimum rate used in their experiment was 0.01 s^{-1}, which was one order of magnitude higher compared to our experiments performed at 0.0017 s^{-1}.

For composites after deformation, the orientation of the scattering signal perpendicularly to the stretching direction was visible. The effect was more pronounced when the nanotube concentration was higher. Looking at the vertical scattering profiles for the non-deformed and deformed the same composite, can be seen the difference. Scattering after deformation is greater. However, when analyzing horizontal profiles, scattering from deformed samples in this direction is smaller. When the scattering was integrated for the whole image, the differences in the total scattering intensity before and after deformation did not exceed 5%, which is not significant. This means that scattering for composites was mainly from the nanotubes, so the shapes of the patterns indicate the orientation of the nanotubes in the direction of deformation. The contribution to the scattering of that coming from the crystalline phase was small. Scattering on nanovoids was not observed.

4. Conclusions

As a result of the conducted research, it was found that the reduction of entanglements of macromolecules in the polylactide-MWCNTs composite affects: filler dispersion during processing, ability to crystallize, and mechanical properties. In the composites in which PLA macromolecules were less entangled, better dispersion of nanoparticles was obtained. This can be attributed to easier penetration of macromolecules into the agglomerated CNTs, as well as lower viscosity in the melt, altering the processing conditions.

Large differences between composites with entangled and less entangled macromolecules were observed during non-isothermal crystallization studies. PLAd prepared from solution had fewer nuclei than PLAi, which limited the normal and cold crystallization in this polymer. The presence of nanotubes in the entangled polymer hindered their crystallization. The potential effect of nucleation on the nanotubes did not outweigh the fact that the nanotubes were an obstacle to crystal growth. The addition of nanoparticles to PLAd, better dispersed than in PLAi, gave a sufficient number of nuclei, which, combined with greater mobility of macromolecules and easier obstacle avoidance, resulted in intensive crystallization already during cooling, not only during cold crystallization.

The isothermal crystallization confirmed the observations from the non-isothermal crystallization that there were fewer nuclei in PLAd, which increased the crystallization time. In composites, the process was faster for those with less entangled macromolecules due to easier migration of macromolecules into the growing crystals.

The influence of macromolecular entanglements as well as the content and dispersion of nanotubes, was visible when examining the mechanical properties. Partial disentanglement of macromolecules in the polylactide matrix resulted in lower stresses during the initiation of the plastic deformation. Although the strain-hardening phase for homopolymers was more pronounced for more entangled PLAi, in composites the stress increased faster in those with more and better-dispersed MWCNTs. The better dispersion of the fillers had a greater effect on the stresses than the degree of entanglement of the macromolecules. The slight increase in volume observed during the deformation of homopolymers was attributed to the formation of a small number of microvoids. WAXS studies confirmed the occurrence of the intensive

strain-induced crystallization of polylactide. The crystals were strongly oriented, especially when the number of nanotubes was limited. The MWCNTs themselves also became oriented during the deformation of the composites.

Acknowledgements

Statutory fund of the Centre of Molecular and Macromolecular Studies, Polish Academy of Sciences is acknowledged.

References

[1] Garlotta D.: A literature review of poly(lactic acid). Journal of Polymers and the Environment, **9**, 63–84 (2001). https://doi.org/10.1023/A:1020200822435

[2] Stoclet G., Seguela R., Lefebvre J. M., Elkoun S., Vanmansart C.: Strain-induced molecular ordering in polylactide upon uniaxial stretching. Macromolecules, **43**, 1488–1498 (2010). https://doi.org/10.1021/ma9024366

[3] Zhang J., Tashiro K., Tsuji H., Domb A. J.: Disorder-to-order phase transition and multiple melting behavior of poly(L-lactide) investigated by simultaneous measurements of WAXD and DSC. Macromolecules, **41**, 1352–1357 (2008). https://doi.org/10.1021/ma0706071

[4] Kaseem M., Hamad K., Deri F., Ko Y. G.: A review on recent researches on polylactic acid/carbon nanotube composites. Polymer Bulletin, **74**, 2921–2937 (2017). https://doi.org/10.1007/s00289-016-1861-6

[5] Gonçalves C., Gonçalves I. C., Magalhães F. D., Pinto A. M.: Poly(lactic acid) composites containing carbon-based nanomaterials: A review. Polymers, **9**, 269 (2017). https://doi.org/10.3390/polym9070269

[6] Kim S. Y., Shin K. S., Lee S. H., Kim K. W., Youn J. R.: Unique crystallization behavior of multi-walled carbon nanotube filled poly(lactic acid). Fibers and Polymers, **11**, 1018–1023 (2010). https://doi.org/10.1007/s12221-010-1018-4

[7] Xu Z., Niu Y., Wang Z., Li H., Yang L., Qiu J., Wang H.: Enhanced nucleation rate of polylactide in composites assisted by surface acid oxidized carbon nanotubes of different aspect ratios. ACS Applied Materials Interfaces, **3**, 3744–3753 (2011). https://doi.org/10.1021/am200932q

[8] Mina M. F., Beg M. D. H., Islam M. R., Nizam A., Alam A. K. M. M., Yunus R. M.: Structures and properties of injection-molded biodegradable poly(lactic acid) nanocomposites prepared with untreated and treated multiwalled carbon nanotubes. Polymer Engineering and Science, **54**, 317–326 (2014). https://doi.org/10.1002/pen.23564

[9] Park S. H., Lee S. G., Kim S. H.: Isothermal crystallization behavior and mechanical properties of polylactide/carbon nanotube nanocomposites. Composites Part A: Applied Science and Manufacturing, **46**, 11–18 (2013). https://doi.org/10.1016/j.compositesa.2012.10.011

[10] Rizvi R., Khan O., Naguib H. E.: Development and characterization of solid and porous polylactide-multiwall carbon nanotube composites. Polymer Engineering and Science, **51**, 43–53 (2011). https://doi.org/10.1002/pen.21792

[11] Wu C-S., Liao H-T.: Study on the preparation and characterization of biodegradable polylactide/multi-walled carbon nanotubes nanocomposites. Polymer, **48**, 4449–4458 (2007) https://doi.org/10.1016/j.polymer.2007.06.004

[12] Zhao Y., Qiu Z., Yan S., Yang W.: Crystallization behavior of biodegradable poly(L-lactide)/multiwalled carbon nanotubes nanocomposites from the amorphous state. Polymer Engineering and Science, **51**, 1564–1573 (2011). https://doi.org/10.1002/pen.21933

[13] Wu D., Wu L., Zhou W., Zhang M., Yang T.: Crystallization and biodegradation of polylactide/carbon nanotube composites. Polymer Engineering and Science, **50**, 1721–1733 (2010). https://doi.org/10.1002/pen.21695

[14] Kuan C-F., Kuan H-C., Ma C-C. M., Chen C-H.: Mechanical and electrical properties of multi-wall carbon nanotube/poly(lactic acid) composites. Journal of Physics and Chemistry of Solids, **69**, 1395–1398 (2008). https://doi.org/10.1016/j.jpcs.2007.10.060

[15] Szatkowski P., Czechowski L., Gralewski J., Szatkowska M.: Mechanical properties of polylactide admixed with carbon nanotubes or graphene nanopowder. Materials, **14**, 5955 (2021). https://doi.org/10.3390/ma14205955

[16] Wu D., Wu L., Zhou W., Sun Y., Zhang M.: Relations between the aspect ratio of carbon nanotubes and the formation of percolation networks in biodegradable polylactide/carbon nanotube composites. Journal of Polymer Science Part B: Polymer Physics, **48**, 479–489 (2010). https://doi.org/10.1002/polb.21909

[17] Ramontja J., Ray S. S., Pillai S. K., Luyt A. S.: High-performance carbon nanotube-reinforced bioplastic. Macromolecular Materials and Engineering, **294**, 839–846 (2009). https://doi.org/10.1002/mame.200900197

[18] Yoon J. T., Jeong Y. G., Lee S. C., Min B. G.: Influences of poly(lactic acid)-grafted carbon nanotube on thermal, mechanical, and electrical properties of poly(lactic acid). Polymers Advanced Technologies, **20**, 631–638 (2009). https://doi.org/10.1002/pat.1312

[19] Mat Desa M. S. Z., Hassan A., Arsad A., Mohammad N. N. B.: Mechanical properties of poly(lactic acid)/multiwalled carbon nanotubes nanocomposites. Materials Research Innovations, **18**, S6-14–S6-17 (2014). https://doi.org/10.1179/1432891714Z.000000000924

[20] Chiu W-M., Chang Y-A., Kuo H-Y., Lin M-H., Wen H-C.: A study of carbon nanotubes/biodegradable plastic polylactic acid composites. Journal of Applied Polymer Science, **108**, 3024–3030 (2008). https://doi.org/10.1002/app.27796

[21] Villmow T., Pötschke P., Pegel S., Häussler L., Kretzschmar B.: Influence of twin-screw extrusion conditions on the dispersion of multi-walled carbon nanotubes in a poly(lactic acid) matrix. Polymer, **49**, 3500–3509 (2008). https://doi.org/10.1016/j.polymer.2008.06.010

[22] Wool R. P.: Polymer entanglements. Macromolecules, **26**, 1564–1569 (1993). https://doi.org/10.1021/ma00059a012

[23] Eckstein A., Suhm J., Friedrich C., Maier R-D., Sassmannshausen J., Bochmann M., Mülhaupt R.: Determination of plateau moduli and entanglement molecular weights of isotactic, syndiotactic, and atactic polypropylenes synthesized with metallocene catalysts. Macromolecules, **31**, 1335–1340 (1998). https://doi.org/10.1021/ma971270d

[24] Fetters L. J., Lohse D. J., Colby R. H.: Chain dimensions and entanglement spacings. in 'Physical properties of polymers handbook' (ed: Mark J. E.) Springer, New York, 447–454 (2007).

[25] Pawlak A.: The entanglements of macromolecules and their influence on the properties of polymers. Macromolecular Chemistry and Physics, **220**, 1900043 (2019). https://doi.org/10.1002/macp.201900043

[26] Wang B., Cavallo D., Zhang X., Zhang B., Chen J.: Evolution of chain entanglements under large amplitude oscillatory shear flow and its effect on crystallization of isotactic polypropylene. Polymer, **186**, 121899 (2020). https://doi.org/10.1016/j.polymer.2019.121899

[27] Kong D-C., Yang M-H., Zhang X-S., Du Z-C., Fu Q., Gao X-Q., Gong J-W.: Control of polymer properties by entanglement: A review. Macromolecular Materials and Engineering, **306**, 2100536 (2021). https://doi.org/10.1002/mame.202100536

[28] Wang X., Liu R., Wu M., Wang Z., Huang Y.: Effect of chain disentanglement on melt crystallization behavior of isotactic polypropylene. Polymer, **50**, 5824–5827 (2009). https://doi.org/10.1016/j.polymer.2009.10.002

[29] Sasaki T., Morino D., Tabata N.: Origin of enhanced cold crystallization rate for freeze-dried poly(L-lactide) from solutions. Polymer Engineering and Science, **51**, 1858–1865 (2011). https://doi.org/10.1002/pen.21977

[30] Liu X-T., Bao R-Y., Li Y-M., Yang W., Xie B-H., Yang M-B.: Effect of chain entanglement on the melt-crystallization behavior of poly(L-lactide) acid. Polymer Research, **23**, 164 (2016). https://doi.org/10.1007/s10965-016-1060-z

[31] Krajenta J., Safandowska M., Pawlak A., Galeski A.: All-polymer composites – A new approach with the use of disentangled semi-crystalline polymers. Part I. Disentangling and properties of disentangled polylactide. Polimery, **65**, 167–173 (2020). https://doi.org/10.14314/polimery.2020.3.1

[32] Sun C., Zheng Y., Xu S., Ni L., Li X., Shan G., Bao Y., Pan P.: Role of chain entanglements in the stereocomplex crystallization between poly(lactic acid) enantiomers. ACS Macro Letters, **10**, 1023–1028 (2021). https://doi.org/10.1021/acsmacrolett.1c00394

[33] Krajenta J., Pawlak A., Galeski A.: All-polymer composites – A new approach with the use of disentangled semi-crystalline polymers. Part II. Preparation of composites from partially disentangled polylactide. Polimery, **65**, 261–267 (2020). https://doi.org/10.14314/polimery.2020.4.1

[34] Barangizi H., Pawlak A.: Crystallization of partially disentangled polypropylene in nanocomposites with aluminum oxide. Polymer, **254**, 125049 (2022). https://doi.org/10.1016/j.polymer.2022.125049

[35] Luo J., Liu M., Chen J., Min J., Fu Q., Zhang J.: Effectively maintaining the disentangled state of isotactic polypropylene in the presence of graphene nanoplatelet. Polymer, **226**, 123806 (2021). https://doi.org/10.1016/j.polymer.2021.123806

[36] Drakopoulos S. X., Tarallo O., Guan L., Martin-Fabiani I., Ronca S.: Nanocomposites of Au/disentangled UHMWPE: A combined optical and structural study. Molecules, **25**, 3225 (2020). https://doi.org/10.3390/molecules25143225

[37] Zhang X., Zhao S., Xin Z.: The chain dis-entanglement effect of polyhedral oligomeric silsesquioxanes (POSS) on ultra-high molecular weight polyethylene (UHMWPE). Polymer, **202**, 122631 (2020). https://doi.org/10.1016/j.polymer.2020.122631

[38] Romo-Uribe A., Reyes-Mayer A., Paredes-Pérez M., Lichtenhan J., Yañez-Lino M., Sarmiento-Bustos E.: POSS driven chain disentanglements, decreased the melt viscosity and reduced O_2 transmission in polyethylene. Polymer, **165**, 61–71 (2019). https://doi.org/10.1016/j.polymer.2019.01.024

[39] Romo-Uribe A.: Dispersion at single unit TiO_2 nanoparticles reduced T_g, induced chain disentanglement and reduced tensile modulus in waterborne acrylic coatings. Macromolecular Materials and Engineering, **306**, 2000591 (2021). https://doi.org/10.1002/mame.202000591

[40] Pawlak A., Galeski A., Rozanski A.: Cavitation during deformation of semicrystalline polymers. Progress in Polymer Science, **39**, 921–958 (2014). https://doi.org/10.1016/j.progpolymsci.2013.10.007

[41] Fischer E. W., Sterzel H. J., Wegner G. K. Z. Z.: Investigation of the structure of solution grown crystals of lactide copolymers by means of chemical reactions. Kolloid-Zeitschrift und Zeitschrift für Polymere, **251**, 980–990 (1973). https://doi.org/10.1007/BF01498927

[42] Saeidlou S., Huneault M. A., Li H., Park C. B.: Poly(lactic acid) crystallization. Progress in Polymer Science, **37**, 1657–1677 (2012). https://doi.org/10.1016/j.progpolymsci.2012.07.005

[43] Barrau S., Vanmansart C., Moreau M., Addad A., Stoclet G., Lefebvre J-M., Seguela R.: Crystallization behavior of carbon nanotube−polylactide nanocomposites. Macromolecules, **44**, 6496–6502 (2011). https://doi.org/10.1021/ma200842n

[44] Zhou C., Li H., Zhang W., Li J., Huang S., Meng Y., deClaville Christiansen J., Yu Z., Wu Z., Jiang S.: Direct investigations on strain-induced cold crystallization behavior and structure evolutions in amorphous poly(lactic acid) with SAXS and WAXS measurements. Polymer, **90**, 111–121 (2016). https://doi.org/10.1016/j.polymer.2016.03.014

[45] Zhang X., Schneider K., Liu G., Chen J., Brüning K., Wang D., Stamm M.: Structure variation of tensile-deformed amorphous poly(L-lactic acid): Effects of deformation rate and strain. Polymer, **52**, 4141–4149 (2011). https://doi.org/10.1016/j.polymer.2011.07.003

[46] Mahendrasingam A., Blundell D. J., Parton M., Wright A. K., Rasburn J., Narayanan T., Fuller W.: Time resolved study of oriented crystallisation of poly(lactic acid) during rapid tensile deformation. Polymer, **46**, 6009–6015 (2005). https://doi.org/10.1016/j.polymer.2005.05.081